SCIENTIFIC REPORTS

OPEN

SUBJECT AREAS:
MECHANICAL PROPERTIES
MECHANICAL ENGINEERING
COMPOSITES
METALS AND ALLOYS

Received
7 February 2014

Accepted
2 May 2014

Published
23 May 2014

Correspondence and requests for materials should be addressed to H.L.Y. (hailiang@uow.edu.au; yuhailiang1980@tom.com)

A deformation mechanism of hard metal surrounded by soft metal during roll forming

Hailiang YU[1,2], A. Kiet TIEU[1], Cheng LU[1], Xiong LIU[1], Ajit GODBOLE[1], Huijun LI[1], Charlie KONG[3] & Qinghua QIN[4]

[1]School of Mechanical, Materials & Mechatronics Engineering, University of Wollongong, NSW 2500, Australia, [2]School of Mechanical Engineering, Shenyang University, Shenyang 110044, China, [3]Electron Microscope Unit, University of New South Wales, Sydney, NSW 2052, Australia, [4]Research School of Engineering, Australian National University, Canberra, ACT 2601, Australia.

It is interesting to imagine what would happen when a mixture of soft-boiled eggs and stones is deformed together. A foil made of pure Ti is stronger than that made of Cu. When a composite Cu/Ti foil deforms, the harder Ti will penetrate into the softer Cu in the convex shapes according to previously reported results. In this paper, we describe the fabrication of multilayer Cu/Ti foils by the roll bonding technique and report our observations. The experimental results lead us to propose a new deformation mechanism for a hard metal surrounded by a soft metal during rolling of a laminated foil, particularly when the thickness of hard metal foil (Ti, 25 μm) is much less than that of the soft metal foil (Cu, 300 μm). Transmission Electron Microscope (TEM) imaging results show that the hard metal penetrates into the soft metal in the form of concave protrusions. Finite element simulations of the rolling process of a Cu/Ti/Cu composite foil are described. Finally, we focus on an analysis of the deformation mechanism of Ti foils and its effects on grain refinement, and propose a grain refinement mechanism from the inside to the outside of the laminates during rolling.

Micromanufacturing has attracted increasing attention over recent years because of consumer-driven and industry-driven trends towards product miniaturization in applications such as automotive engineering and medicine[1,2]. The global market for Micro Systems Technology (MST) and Micro Electro Mechanical Systems (MEMS) reached $52 billion in 2009. The MEMS market is expected to grow from $11 billion in 2012 to $22.5 billion in 2018, and the BioMEMS market is expected to expand from $1.9 billion in 2012 to $6.6 billion in 2018[3]. Most of these products contain mechanical parts produced by microforming, a significant manufacturing process that involves the fabrication of products from ultrathin foils. The growing demand on micromanufacturing to produce "smaller" and "smarter" micro parts requires the foils to have superior properties and characteristics in terms of thickness, functionality, and formability.

Metallic nanocomposite materials have attracted increasing attention due to their potential in design for novel applications using advanced materials. This is due to their high plastic flow strength and indentation hardness, better ductility, greater radiation damage resistance, improved electrical and magnetic properties, and enhanced fatigue failure resistance compared to conventional metallic materials[4–8]. Valiev *et al.*[9] reported that there are more than 100 specific market areas with demand for nanostructured metals. Due to the huge potential application of metallic nanostructured materials, a number of Severe Plastic Deformation (SPD) techniques such as High Pressure Torsion (HPT)[10], Equal Channel Angular Pressing (ECAP)[11] and Accumulative Roll Bonding (ARB)[12,13] have been developed to produce metallic nanocomposite materials. Among these SPD techniques, the ARB technique is suitable for production of metallic nanostructured laminates.

In recent years, metal laminates have become increasingly popular for engineering applications since they usually possess characteristic properties suitable for special service performance[14–18]. It has been shown that the Roll Bonding (RB) and ARB techniques can be successfully used to produce multi-component materials with tailored properties by reinforcement or grading. This allows optimization of the properties of products based on two or more alloys[19]. The RB and ARB techniques have been used to fabricate products containing composite laminates with materials such as Cu/Nb[4], Al/Al_2O_3/SiC[20], Al/Cu[21], Al/Mg[22], Ti/Nb[23], Cu/Ni[24], Cu/Si[25], Al/Ni[26], Al/Steel[27], etc. In addition, the Asymmetric Rolling (AR) technique has been used to produce bimetallic sheets and

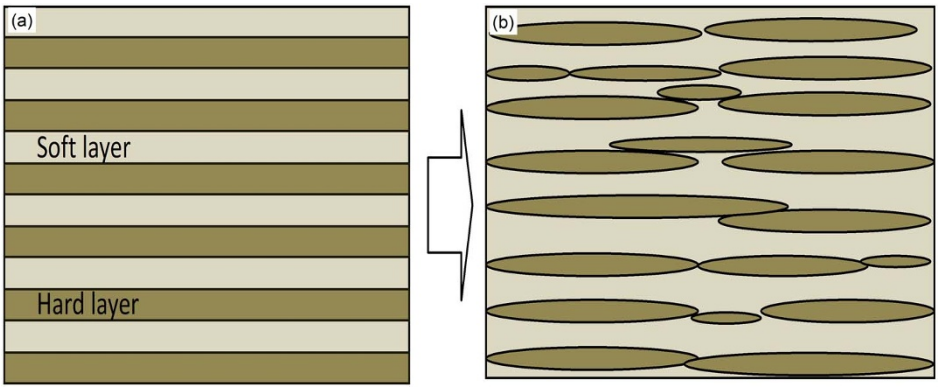

Figure 1 | **Illustration of deformation feature of laminate with increasing strain during rolling, (a) after the first pass, (b) after multi rolling pass.**

foils[28,29]. It was seen that the shear friction during AR had a direct impact on the stress state of the metal, and that cross shear had the most influence on metal flow and improved the bonding strength. To improve the properties of such materials, one major goal is to synthesize nanostructured composites with a uniform microstructure and a homogeneous distribution of reinforcing constituents in the matrix on the micro- or nano-scale[13] in bulk form. However, when stress discontinuities occur at the planar interface between two immiscible materials, instabilities can appear due to interfacial and bulk diffusion or dislocation mobility[30,31]. Thus, the deformation of each layer during the rolling process is a key mechanism that controls the material properties. In previous studies[32–35], it was observed that during laminated rolling of metals with different mechanical properties and involving high reduction in thickness, a plastic instability develops and the harder phase starts necking, gets separated and finally fractures to similar oval-shaped segments, as shown in Fig. 1.

During heat treatment, the metallic laminated materials will transform into metal-intermetallic laminated composites[36], which also offer an attractive combination of properties such as high toughness coupled with low density, and high oxidation resistance of the intermetallics[37]. These desirable properties are due to their mixed bonding, which is part covalent, part metallic and part ionic[38]. Metal-intermetallic laminates have the potential to perform various functions, such as ballistic protection, heat exchange, blast mitigation

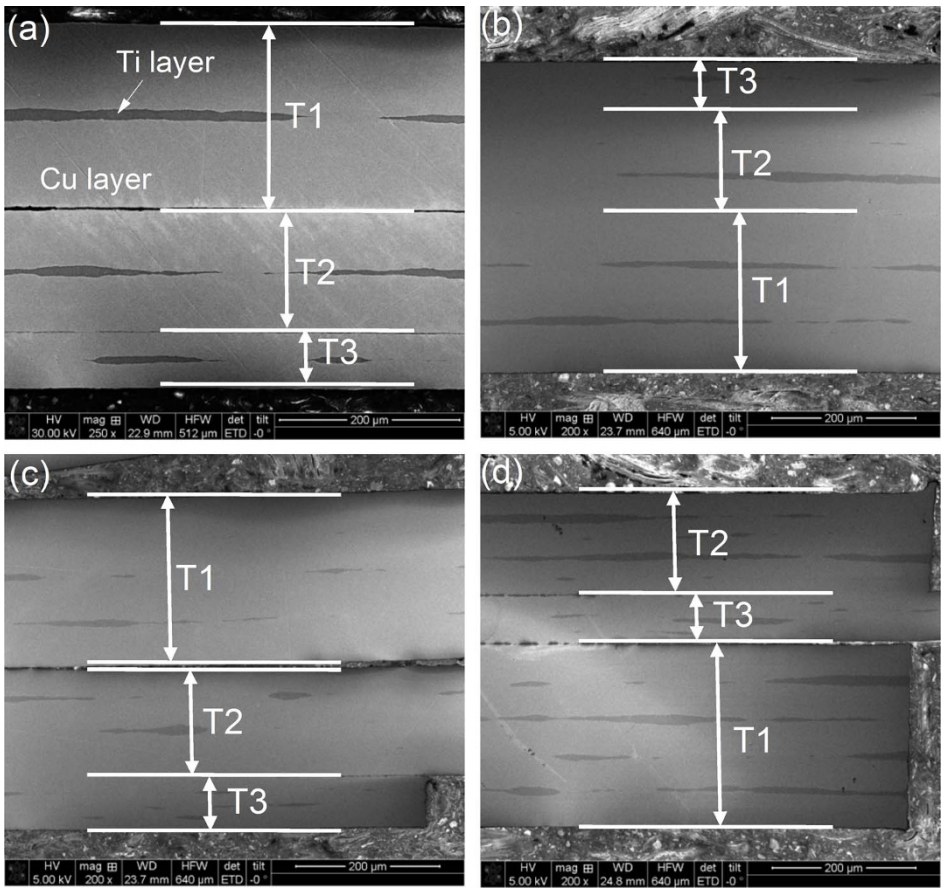

Figure 2 | **SEM image of the section of Cu/Ti nanocomposite foils with different thickness for (a) one layer, (b) two layers, (c) three layers and (d) four layers Ti foils.**

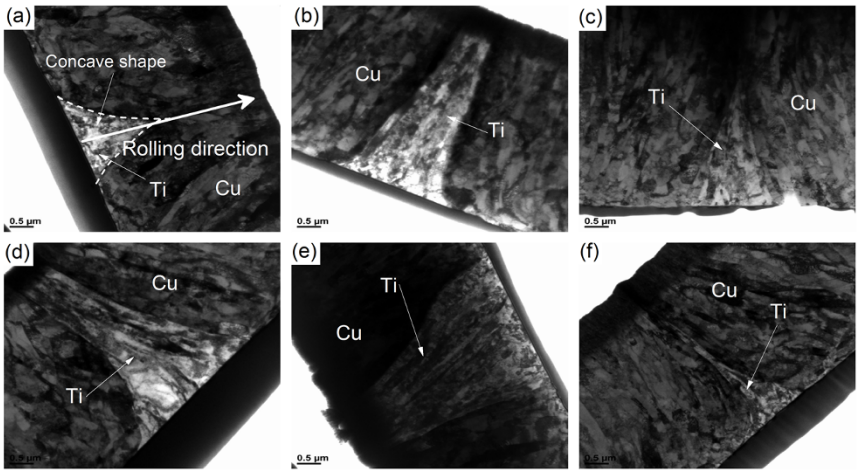

Figure 3 | **TEM graph of Ti layer shape along the rolling direction.**

and vibration damping[39]. The unique physical properties of intermetallic titanium-copper (TiCu), which is one kind of functional material[40], such as extreme hardness, good sound absorption, electric conductivity *etc*., make this alloy a subject of scientific and technological interest. In addition, TiCu alloys are now receiving a great deal of attention as ultra-high strength and conductive materials for applications such as conductive springs, interconnections *etc*[41].

In this study, we have applied the cold roll-bonding technique to produce nanocomposite Cu/Ti foils which can be used to fabricate smarter micro parts with high strength, good thermal conductivity and sound absorption properties. From the experimental results, we found that the hard Ti foil material fractures and is distributed in the Cu matrix during rolling. We also propose a deformation mechanism of the hard layer surrounded by soft materials during rolling which is different to that shown in Fig. 1.

Results

SEM micrograph of Cu/Ti foils. Fig. 2 shows Scanning Electron Microscope (SEM) images of a section of Cu/Ti laminates with different foil thicknesses. Fig. 2a shows the Cu/Ti/Cu foil, Fig. 2b Cu/Ti/Cu/Ti/Cu foil, Fig. 2c Cu/Ti/Cu/Ti/Cu/Ti/Cu foil and Fig. 2d Cu/Ti/Cu/Ti/Cu/Ti/Cu/Ti/Cu foil. As seen in the figure, the Ti layers become increasingly discontinuous in the Cu matrix as the laminate foil thickness reduces. In the case of annealed Cu and Ti foils, the yield strength of the Ti layer is higher than that of the Cu layer. These experimental results are similar to the observation in Refs [32–35], in that the hard layers exhibit necking and fracture. However, there has been no analysis of the mechanism of the phenomenon to date. We generally would expect the hard material to break the softer material, when they undergo deformation together. However, the experimental observations are contrary to this expectation. We need to explain why the hard materials fractured in rolling when surrounded by soft material.

TEM images of Cu/Ti interface. Fig. 3 shows TEM (Transmission Electron Microscope) images of different sections around the fracture end of Ti layer for rolled foils. It can be seen that all the Cu/Ti interfaces are 'concave' when observed from the Ti side, in which the Cu layers are recessed into the Ti layers. It is obvious that this is different from Fig. 1, in which the interfaces are convex when observed from the hard metal side.

Grain refinement during rolling. Fig. 4 shows TEM images of the microstructure of Cu near the interface with different laminate foil thickness with one layer Ti foil. When the laminate foil thickness is reduced to 220 μm, the grain size near the Ti layer is much finer than elsewhere. This implies severe shear friction deformation between the Ti layer and the Cu layer during rolling, as shown in Fig. 4a. With

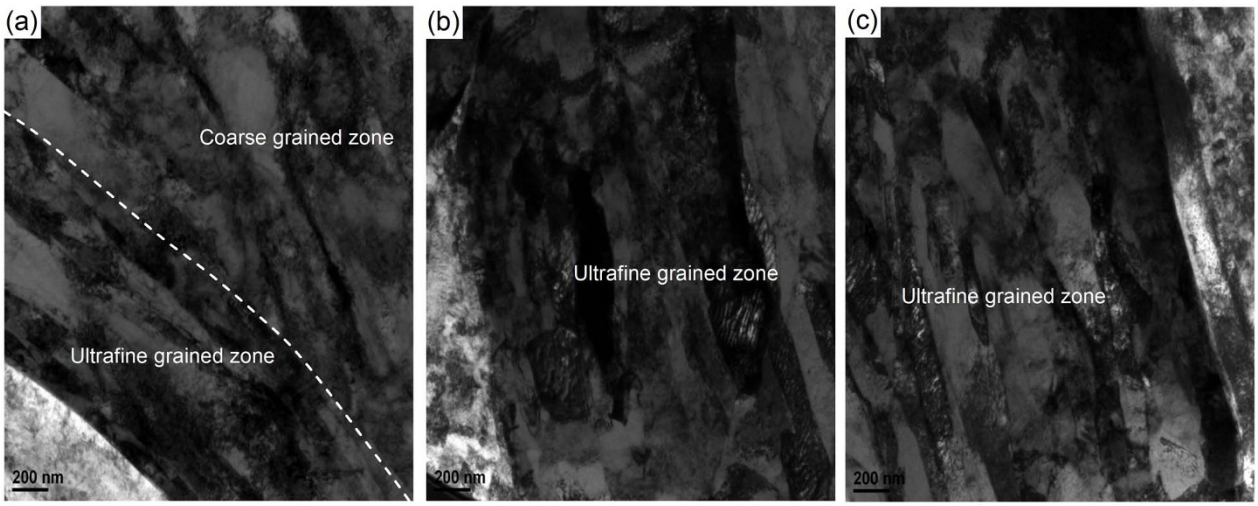

Figure 4 | **TEM graph of microstructure of Cu layer near interface with the laminate foil thickness 220 μm (a), 140 μm (b) and 62 μm (c).**

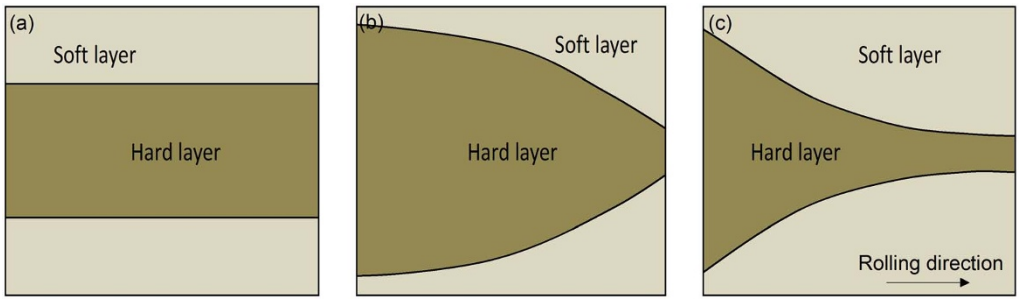

Figure 5 | Illustration of interface shapes between hard and soft layers. (a) uniform deformation; (b) convex shape; (c) concave shape.

further reduction in the foil thickness, the strain in the foil increases and the microstructure of Cu layer is nearly uniform, as shown in Fig. 4c. The strength of nanostructured metal materials is usually related to the grain size by the well-known Hall-Petch relationship:

$$\sigma_y = \sigma_0 + kd^{-0.5} \quad (1)$$

where σ_y is yield stress, σ_0 and k are constants for the material, and d is the grain size. With reduced grain size of Cu near the Ti layer, the strength of the Cu in this zone will be higher than elsewhere. As the number of rolling passes increases, the thickness of the refined layer gradually increases and finally becomes uniform. This may be one of the main grain refinement mechanisms of nanocomposite foil materials fabricated by the rolling technique.

Discussion

For fabrication of high quality nanocomposite foils, deformation of the harder material is very important for grain refinement. We used a Ti foil to enhance the Cu matrix. The thickness of Ti foil is 1/12 of the thickness of the Cu foil. Generally, we would expect the Cu and Ti layers to deform uniformly in the rolling process, eventually resulting in a laminate structure. Under ideal conditions, for two layers with the same mechanical properties, we expect the interface to be a straight line, as shown in Fig. 5a. However, this may not be true in the case of Cu and Ti foils, due to different mechanical properties of Cu and Ti. Some researchers have investigated the conditions under which thicknesses of the hard layer and the soft layer are the same or similar. Mozaffari *et al.*[33] studied the structure of multilayered Al/Ni composite during ARB. They observed that after the first cycle of sandwich production, the nickel layers were bonded with the aluminum layer. Then they started to neck and fractured locally. After six cycles, the nickel layer broke up and was homogenously distributed in the aluminum matrix. Su *et al.*[34] studied the structure of multilayered AA6061/AA1050 aluminum composite fabricated by ARB. Their observations were similar to those of Mozaffari *et al.* During the first three cycles, the hard layers (AA6061) were able to deform in the same way as the soft layers (AA1050). The deformation became inhomogeneous and the thickness of hard layers starts to vary along the rolling direction after subsequent ARB cycles. The hard layers started to neck with further deformation and the adjacent soft material then protruded and filled the necked and fractured regions. In the results of Mozaffari *et al.* and Su *et al.*, the interface shape of hard layer was seen to be similar to that in Fig. 5b, as well as the illustration by Junqua and Grillé[31]. However, in this study, it was found that when the thickness of the hard layer is much thinner than that of the soft layer, new deformation pattern develops, where the hard layer assumes a concave shape, as shown in Fig. 5c and Fig. 3.

In Refs [32–35], the thickness of the soft layers is the same as that of the hard layers. In the deformation process, the hard layer plays a key role which results in the soft layer surrounding the hard layer material. However, in the present study, the thickness of the Ti layer is only 25 μm, and the thickness of Cu layer is 300 μm. In the deformation process, the thicker Cu layer plays the key role. In recent years, size effects on the plasticity of materials have attracted increasing attention[42–45]. Fig. 6 shows FE-simulation results of the Ti layer shape for different thicknesses of the Ti layer. It is seen that when the thickness of Ti layer is 200, 100 or 50 μm, the interface shape of the Ti layer is convex, which is similar with the observation in Refs [32–35]. When the thickness of the Ti layer is reduced to 25 μm, the interface of the Ti layer adopts a concave shape. Fig. 7 shows the equivalent stress and strain distribution in the Cu/Ti laminate with one layer Ti foil in the rolling deformation zone simulated by FEM. In Fig. 7a and 7b, it is seen that we can associate a wavelength to the deformation of the laminate. The fluctuation wavelength of laminate layers under instability deformation conditions studied by Junqua and Grilhé[31,46], was affected by the elastic modulus, yield stress, thickness, and surface energy, as shown in equations (2)–(8).

$$F(hK)/hK \geq \gamma/4Ch \quad (2)$$

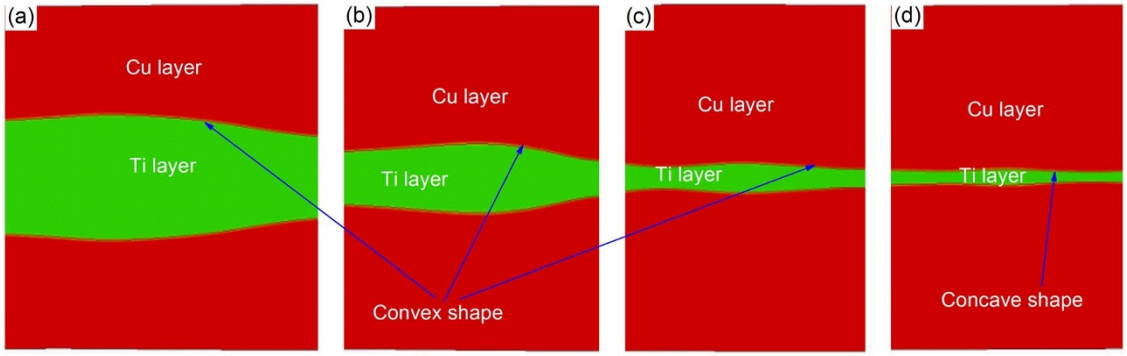

Figure 6 | FE simulation of Ti layer shape after rolling processing for Ti layer thickness (a) 200 μm, (b) 100 μm, (c) 50 μm, and (d) 25 μm.

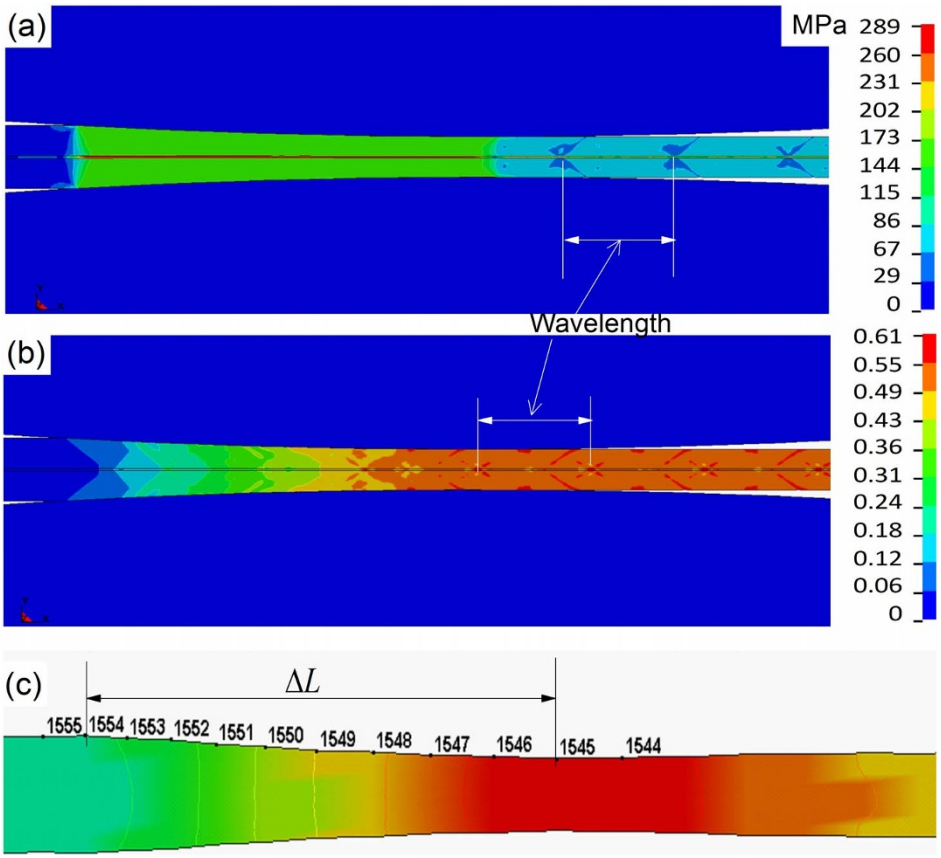

Figure 7 | Equivalent stress (a), strain (b) distribution of the laminate foil in the rolling deformation zone, and sectioned wavelength (c).

$$F(hK)=(1-\Gamma)(1+K)\frac{K(1-\Gamma^2)+\exp(-2hK)[D+4hK\Gamma(\Gamma-1)]+\exp(-4hK)(D+\Gamma^2K)}{(\Gamma+K)(1+\Gamma K)+4hK\exp(-2hK)(\Gamma+K)(1-\Gamma)-\exp(-4hK)K(1-\Gamma)^2} \quad (3)$$

$$\Gamma=E_B/E_A \quad (4)$$

$$K=\frac{2\pi}{\lambda} \quad (5)$$

$$D=4\Gamma+2K+2\Gamma K \quad (6)$$

$$C=\frac{E_A}{E_B}\left(\frac{7-K}{1+K}\right)^2\left(\frac{\delta a}{a}\right)^2 \quad (7)$$

$$\frac{\delta a}{a}=(\sigma_B-\sigma_A)\frac{E_A+E_B}{2E_AE_B} \quad (8)$$

where λ is the fluctuation wavelength, h is the thickness of Ti layer, E_A is the elastic modulus of the Ti layer, E_B is the elastic modulus of the Cu layer, γ is the isotropic surface energy per unit area (207 mJ/m^2 for pure Ti[47]), σ_A is the yield stress of the Ti layer,

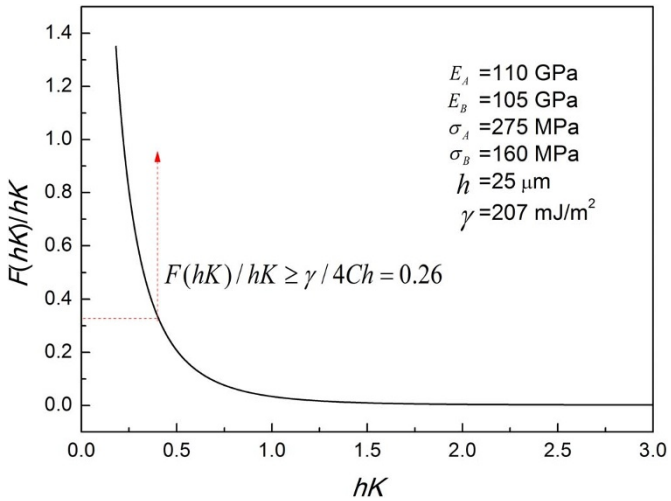

Figure 8 | Representation of $F(hK)/hK$ vs hK curve for h = 25 μm and Γ = 105 : 110.

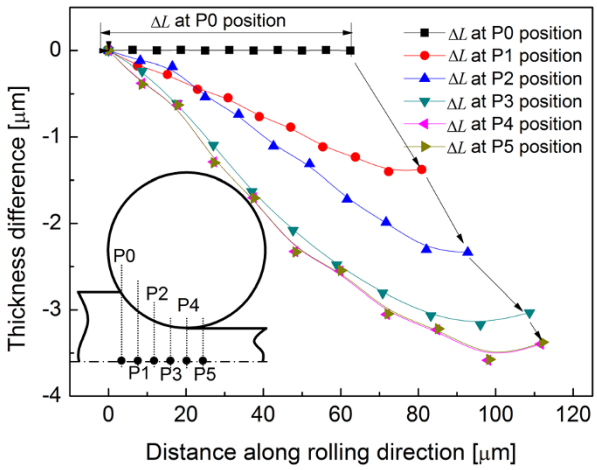

Figure 9 | Evolution of interface of nodes (ΔL) in Figure 7 (c) in the rolling deformation zone.

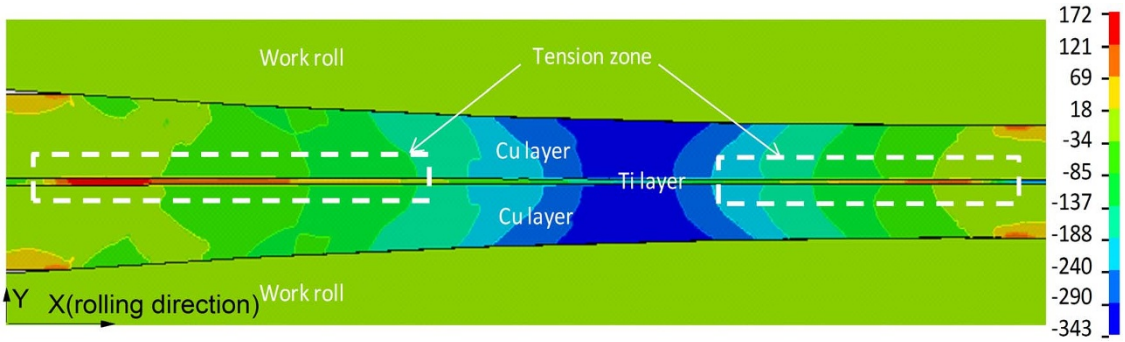

Figure 10 | σ_X **distribution in the rolling deformation zone [MPa].**

and σ_B is the yield stress of the Cu layer. Using the same material parameters in the FE models, the $F(hK)/hK$ vs hK curve for the 25 μm thick Ti layer is shown in Fig. 8. From Eq. (5), the fluctuation wavelength (λ) is about 525 μm, which is close to the FEM-calculated value of 660 μm in Fig. 7. This also corresponds to the length of the Ti layer after the first rolling pass of the Cu/Ti/Cu laminate shown in Fig. 2a. The difference between the analytical result and the FEM may be due to the assumptions of the analytical models which do not consider the thickness effect of the Cu layer. As shown in Fig. 7c, when the Ti layer thickness is 25 μm, the Ti layer has a wavy 'dog-bone' shape, with a large reduction in thickness at some locations. If the reduction of thickness of the Ti layer is caused by compression between Cu layers, the thickness of the Ti layer is seen to be uniform. Thus, it is obvious that the tensile stress along the rolling direction in the deformation zone plays an important role in the deformation mechanism of the Ti layer. Fig. 9 shows the evolution of the interface shape in the rolling process. At the "P0" position (entry point), there is no difference in the foil thicknesses. At the "P1" position, the Ti layer begins to deform, but assumes a convex shape. With increased deformation, the convex shape gradually changes to concave, as at "P2". With further deformation to "P3" and "P4", the interface shape totally transforms into a concave shape.

Fig. 10 shows the σ_X (stress) distribution in the Cu/Ti foil in the rolling deformation zone. At the entry and exit zones, the Ti layer experiences tensile stress because the Cu layers are relatively soft compared with the Ti layer. In the deformation process, the soft Cu foil is more elongated along the rolling direction compared to the hard Ti foil, which develops shear friction force (f_s). The shear stress acting on the Ti layer surfaces makes the Ti layer behave like tensile test samples. When the shear stress is larger than a certain value, the Ti layer undergoes necking. As the number of rolling passes increases, the Ti layer may fracture and become discontinuous as shown in Fig. 2. In addition, this deformation feature also results in severe shear strain at the interface of Cu layers and brings about grain refinement, as shown in Fig. 4a. In the Cu layer, there is a gradient of grain size, with the maximum refinement near the interface of Ti layer/Cu layer. With further rolling deformation, the ultrafine grained zone gradually increases in size. For the rolling process of laminates with a hard metal surrounding soft metals, grain refinement occurs firstly inside the laminates and gradually extends to the laminate surface, as illustrated in Fig. 11.

To fabricate nanocomposite Cu/Ti foils, it is desirable that the Ti layers are uniformly distributed between the Cu layers. A suitable process should be designed to achieve this. From the experimental results, we also found that the Ti layer may have a larger plasticity under the rolling conditions, as shown in Fig. 12. During rolling, the Ti foil is acted upon by two compressive stresses and one tensile stress. Under such conditions, the thickness of Ti layer was reduced from 25 μm to about 200 nm. This suggests a significant enhancement in plasticity, which was 125 times the normal elongation under similar rolling conditions.

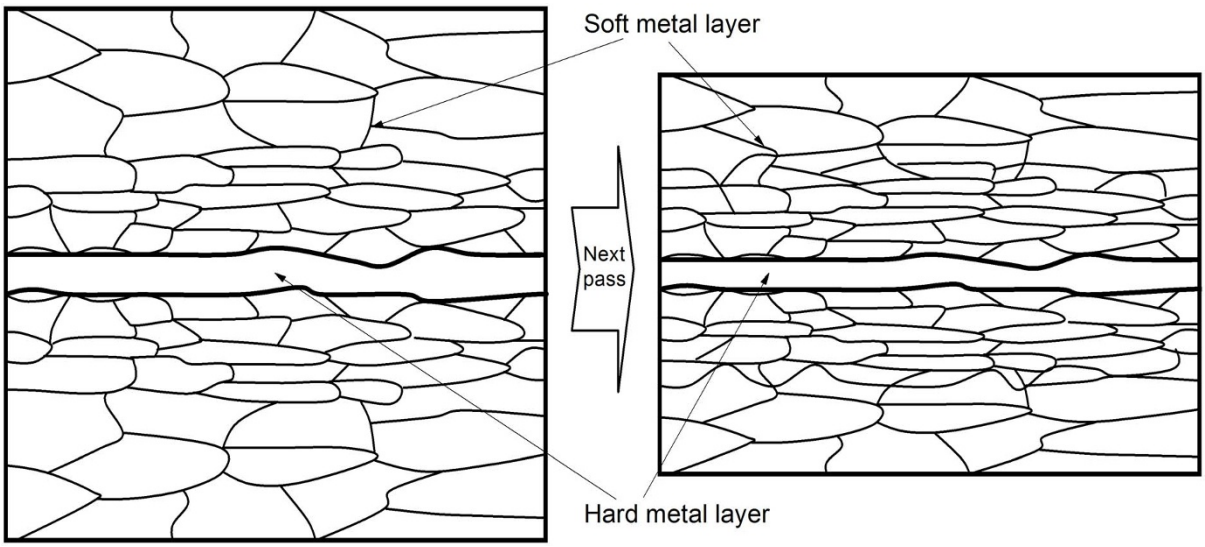

Figure 11 | **Illustration of grain refinement for the hard metal surrounded by soft metal during roll bonding.**

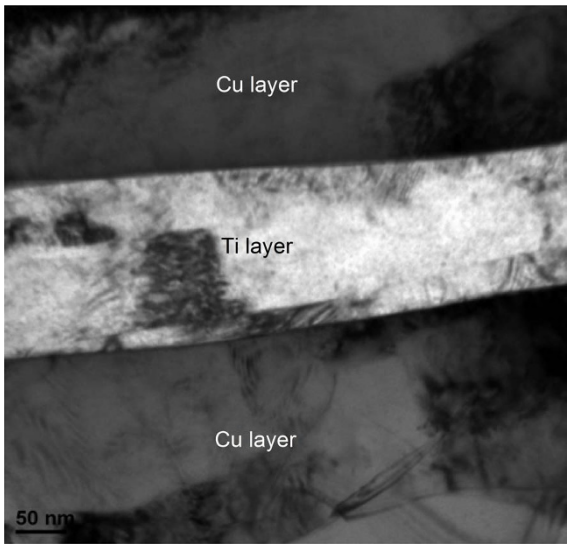

Figure 12 | TEM graph of Ti foil.

In summary, in this study, we fabricated Cu/Ti foils with the thickness up to 70 μm. We discovered a deformation pattern between hard and soft materials, in which the hard Ti layer interface assumes a concave interface shape. With decreasing thickness of the hard layer, the shear friction at the interface between hard and soft layers plays important action in the deformation processing. Due to shear friction between the soft and the hard layers, the grain refinement of the laminates might be developed from the inside to the outside of material during rolling.

Methods

Experimental investigation. Commercial annealed pure Cu foils and annealed Ti foils were used. The Cu foil thickness was 300 μm and the Ti foil thickness was 25 μm. Four kinds of Cu/Ti laminate foils - Cu/Ti/Cu, Cu/Ti/Cu/Ti/Cu, Cu/Ti/Cu/Ti/Cu/Ti/Cu, and Cu/Ti/Cu/Ti/Cu/Ti/Cu/Ti/Cu were fabricated. Fig. 13 shows an illustration of the Cu/Ti laminate rolling process, for (a) single-layer Ti foil, and (b) four-layer Ti foil. The cold rolling process was carried out using a four-high rolling mill with a 120 mm diameter backup roll and a 50 mm diameter work roll. Initially, the Cu sheets and Ti foils were stacked together and welded at one end to prevent slippage. The composite sheets were rolled to about 230 μm, 150 μm and 70 μm as listed in Table 1.

Table 1 | Thickness of laminate foils after cold rolling processing

Number of Ti foil layers in samples		1 layer	2 layer	3 layer	4 layer
Thickness of foils after rolling	T1, μm	220	230	230	240
	T2, μm	140	150	150	147
	T3, μm	62	74	74	70

Scanning Electron Microscopy (SEM) was used primarily to observe details of the layer distribution in samples under a certain thickness. The samples were cut along the TD-ND direction. The morphology of the rolled Cu/Ti foils was studied with a Zeiss Auriga Field Emission Scanning Electron Microscope (FESEM) operating at 20 kV. The RD-ND plane of the rolled samples was employed to carry out the TEM imaging. An FEI xT Nova Nanolab 200 Dual-beam workstation was used to prepare thin-foil specimens from the samples for further TEM observation. The specimens were placed on a standard carbon film Cu grid using an ex-situ lift-out method. A Philips CM200 Field Emission Gun Transmission Electron Microscope (FEG/TEM) equipped with a Bruker Energy Dispersive X-ray (EDAX) Spectroscopy system operating at an accelerating voltage of 200 kV was used to investigate the details of the microstructure.

Modelling. In order to understand better the deformation mechanism of laminate rolling process, FEM simulations were carried out. The FEM technique has been widely used to study the deformation features of workpieces during rolling[48,49], and also to simulate the bimetallic material rolling process[12]. Because the 'concave' Ti layer appears in all samples after rolling as shown in the experimental results, the deformation of the Cu/Ti/Cu laminate foil during only the first pass was simulated using ANSYS/LS-DYNA. In the simulation, the input parameters reflected the experimental conditions. The thickness of the Cu layer was 300 μm, and the Ti foil thicknesses were 25, 50, 100 and 200 μm respectively. The friction coefficient between the sheet and the roll was set as 0.36[50]. During the rolling process, the rolls were regarded as perfectly rigid. Isotropic material models were used for the Cu and Ti layers. The yield stresses for Cu and Ti layers were assumed to be 160 MPa and 275 MPa respectively. The elastic moduli for the Cu and Ti layers were assumed to be 105 GPa and 110 GPa respectively. In the two-dimensional FE simulation, the temperature change and lateral spread of the sheets were neglected. The rolls were assumed to rotate with a constant angular speed. The Cu/Ti/Cu foil was assumed to enter the rolls gap with an initial velocity and exit under the action of the friction force.

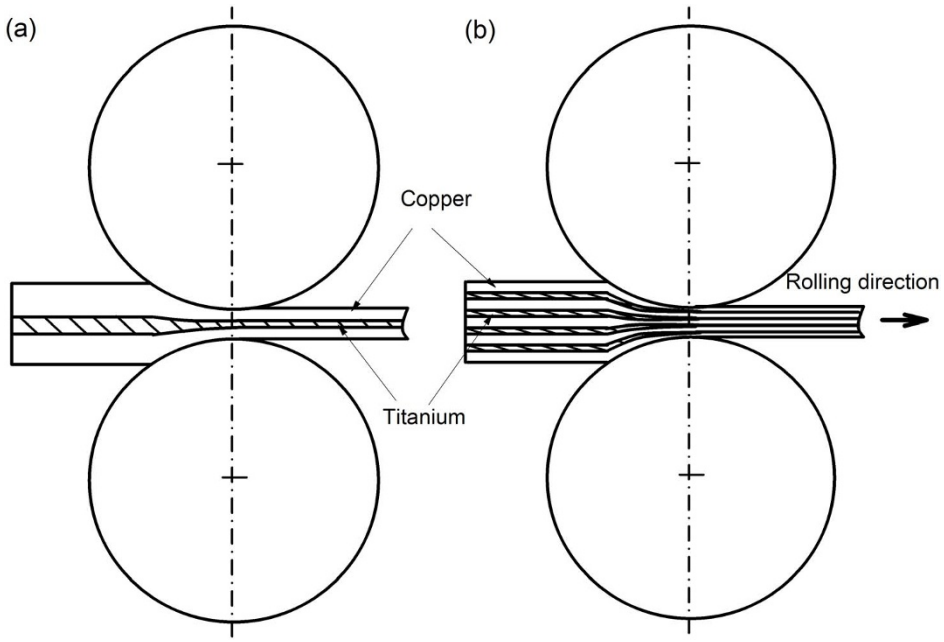

Figure 13 | Illustration of Cu-Ti laminate foils rolling process, (a) one layer Ti foil; (b) four layers Ti foils.

1. Longtin, R., Hack, E., Neuenschwander, J. & Janczak-Rusch, J. Benign joining of ultrafine grained aerospace aluminum alloys using nanotechnology. *Adv. Mater.* **23**, 5812–5816 (2011).
2. Fu, M. W. & Chan, W. L. A review on the state-of-the-art microforming technologies. *Int. J. Adv. Manuf. Technol.* **67**, 2411–2437 (2013).
3. Yole, D. Status of the MEMS industry 2013. (2013) http://www.researchandmarkets.com/reports/2610209/status_of_the_mems_industry_2013 accessed 17.01.2014.
4. Hansen, B. L. *et al.* Modeling the texture evolution of Cu/Nb layered composites during rolling. *Int. J. Plasticity* **49**, 71–84 (2013).
5. Lee, J. H. *et al.* High strain rate deformation of layered nanocomposites. *Nat. Commun.* **3**, 1164 (2012).
6. Zhang, S. J. *et al.* High-strength and thermally stable bulk nanolayered composites due to twin-induced interfaces. *Nat. Commun.* **4**, 1696 (2013).
7. Liu, X. C., Zhang, H. W. & Lu, K. Strain-induced ultrahard and ultrastable nanolaminated structure in Nickel. *Science* **342**, 337–340 (2013).
8. Hao, S. J. *et al.* A transforming metal nanocomposite with large elastic strain, low modulus, and high strength. *Science* **339**, 1191–1194 (2013).
9. Valiev, R. Z., Sabirov, I., Zhilyaev, A. P. & Langdon, T. G. Bulk nanostructured metals for innovative applications. *JOM* **64**, 1134–1142 (2012).
10. Bachmaier, A., Kerber, M., Setman, D. & Pippan, R. The formation of supersaturated solid solutions in Fe-Cu alloys deformed by high-pressure torsion. *Acta Mater.* **60** (3), 860–871 (2012).
11. Mirab, S. & Nili-Ahmadabadi, M. On the flow and mechanical behavior of Al matrix composite reinforced by nickel based (90% Ni-10% Cr) wires during equal channel angular pressing. *Mater. Sci. Eng. A* **583**, 43–51 (2013).
12. Yu, H. L. *et al.* Fabrication of ultra-thin nanostructured bimetallic foils by Accumulative Roll Bonding and Asymmetric Rolling. *Sci. Rep.* **3**, 2373 (2013).
13. Yu, H. L., Lu, C., Tieu, K. & Kong, C. Fabrication of ultrafine-grained Aluminum sheets by four-layer accumulative roll bonding. *Mater. Manuf. Process.* **29**, 448–453 (2014).
14. Bachmaier, A. & Pippan, R. Generation of metallic nanocomposites by severe plastic deformation. *Int. Mater. Rev.* **58**, 41–62 (2013).
15. Yang, J. J. *et al.* Memristive switching mechanism for metal/oxide/metal nanodevices. *Nature Nanotechnol.* **3**, 429–433 (2008).
16. Zbib, H. M., Overman, C. T., Akasheh, F. & Bahr, D. Analysis of plastic deformation in nanoscale metallic multilayers with coherent and incoherent interfaces. *Int. J. Plasticity* **27**, 1618–1639 (2011).
17. Atrian, A. & Fereshteh-Saniee, F. Deep drawing process of steel/brass laminated sheets. *Compos. Part B Eng.* **47**, 75–81 (2013).
18. Viswanathan, V., Laha, T., Balani, K., Agarwal, A. & Seal, S. Challenges and advances in nanocomposite processing techniques. *Mater. Sci. Eng. R* **54**, 121–285 (2006).
19. Bagherzadeh, S., Mollaei-Dariani, B. & Malekzadeh, K. Theoretical study on hydro-mechanical deep drawing process of bimetallic sheets and experimental observations. *J. Mater. Process. Technol.* **212**, 1840–1849 (2012).
20. Ahmadi, A., Toroghinejad, M. R. & Najafizadeh, A. Evaluation of microstructure and mechanical properties of Al/Al2O3/SiC hybrid composite fabricated by accumulative roll bonding process. *Mater. Des.* **53**, 13–19 (2014).
21. Toroghinejad, M. R., Jamaati, R., Dutkiewicz, J. & Szpunar, J. A. Investigation of nanostructured aluminum/copper composite produced by accumulative roll bonding and folding process. *Mater. Des.* **51**, 274–279 (2013).
22. Chang, H. *et al.* Texture evolution of the Mg/Al laminated composite fabricated by the accumulative roll bonding. *Scr. Mater.* **61**, 717–720 (2009).
23. Tohidi, A. A., Ketabchi, M. & Hasannia, A. Nanograined Ti-Nb microalloy steel achieved by Accumulative Roll Bonding (ARB) process. *Mater. Sci. Eng. A* **577**, 43–47 (2013).
24. Eslami, A. H., MojtabaZebarjad, S. & Moshksar, M. M. Study on mechanical and magnetic properties of Cu/Ni multilayer composite fabricated by accumulative roll bonding process. *Mater. Sci. Technol.* **29**, 1000–1005 (2013).
25. Miyajima, Y., Abe, H., Fujii, T., Onaka, S. & Kato, M. Effects of Si on mechanical properties and microstructure evolution in ultrafine-grained Cu-Si alloys processed by accumulative roll bonding. *Acta Mater.* **61**, 1537–1544 (2013).
26. Stover, A. K. *et al.* An analysis of the microstructure and properties of cold-rolled Ni, Al laminate foils. *J. Mater. Sci.* **48**, 5917–5929 (2013).
27. Tayyebi, M. & Eghbali, B. Processing of Al/304 stainless steel composite by roll bonding. *Mater. Sci. Technol.* **28**, 1414–1419 (2012).
28. Li, X. B., Zu, G. Y., Ding, M. M., Mu, Y. L. & Wang, P. Interfacial microstructure and mechanical properties of Cu/Au clad sheet fabricated by asymmetrical roll bonding and annealing. *Mater. Sci. Eng. A* **529**, 485–491 (2011).
29. Pan, S. C., Huang, M. N., Tzou, G. Y. & Syu, S. W. Analysis of asymmetrical cold and hot bond rolling of unbounded clad sheet under constant shear friction. *J. Mater. Process. Technol.* **177**, 114–120 (2006).
30. Semiatin, S. L. & Piehler, H. R. Deformation of sandwich sheet materials in uniaxial tension. *Metall. Trans. A* **10**, 85–96 (1979).
31. Junqua, N. & Grilhé, J. Interface instabilities of multilayers and flat precipitates. *Phil. Mag. A* **71**, 1125–1134 (1995).
32. Mahdavian, M. M., Ghalandari, L. & Reihanian, M. Accumulative roll bonding of multilayered Cu/Zn/Al: An evaluation of microstructure and mechanical properties. *Mater. Sci. Eng. A* **579**, 99–107 (2013).
33. Mozaffari, A., Danesh Manesh, H. & Janghorban, K. Evaluation of mechanical properties and structure of multilayered Al/Ni composites produced by accumulative roll bonding (ARB) process. *J. Alloy. Comp.* **489**, 103–109 (2010).
34. Su, L. H., Lu, C., Tieu, K., Deng, G. Y. & Sun, X. D. Ultrafine grained AA1050/AA6061 composite produced by accumulative roll bonding. *Mater. Sci. Eng. A* **559**, 345–351 (2013).
35. Cui, X. P. *et al.* Influence of raw material selection and fabrication parameters on microstructure and properties of micro-laminated TiB2-TiAl composite sheets. *Mater. Sci. Eng. A* **589**, 83–88 (2014).
36. Dziadon, A., Konieczny, M., Gajewski, M., Iwan, M. & Rzaczynska, Z. Microstructure evolution at the Cu-Ti interface during high temperature synthesis of copper-intermetallic phases layered composite. *Arch. Metall. Mater.* **54**, 455–466 (2009).
37. Konieczny, M. Processing and microstructural characterization of laminated Ti-intermetallic composites synthesized using Ti and Cu foils. *Mater. Lett.* **62**, 2600–2602 (2008).
38. Gschneidner, K. *et al.* A family of ductile intermetallic compounds. *Nature Mater.* **2**, 587–591 (2003).
39. Vecchio, K. S. Synthetic multifunctional metallic-intermetallic laminate composites. *JOM* **57**, 25–31 (2005).
40. Kucheryavyi, O. V., Bratanich, T. I., Skorokhod, V. V., Kopylova, L. I. & Krapivka, N. A. Structural and phase mechanism and rate of interaction between TiCu, Ti_3Cu_4, and Ti_2Cu_3 intermetallic compounds and hydrogen. I. formation and decomposition of intermetallic hydrides. *Powder Metall. Metal Ceram.* **51**, 234–242 (2012).
41. Sharma, G., Sharma, V., Mishra, M. C., Dhaka, M. S. & Sharma, B. K. Electron momentum density distribution in TiCu. *Intermetallics* **19**, 660–670 (2011).
42. Yu, Q. *et al.* Strong crystal size effect on deformation twinning. *Nature* **463**, 335–338 (2010).
43. Ward, D. K. *et al.* Engineering size-scaling of plastic deformation in nanoscale asperities. *Proc. Natl. Acad. Sci. U. S. A.* **106**, 9580–9585 (2009).
44. Shan, Z. W., Mishra, R. K., Asit, S. A. S., Warren, O. L. & Minor, A. M. Mechanical annealing and source-limited deformation in submicrometre-diameter Ni crystals. *Nature Mater.* **7**, 115–119 (2008).
45. Uchic, M. D., Dimiduk, D. M., Florando, J. N. & Nix, W. D. Sample dimensions influence strength and crystal plasticity. *Science* **305**, 986–989 (2004).
46. Junqua, N. & Grilhé, J. Instabilities of planar interfaces between two stressed materials. *Phil. Mag.Lett.* **69**, 61–70 (1994).
47. Jiang, Q. & Lu, H. M. Size dependent interface energy and its applications. *Surf. Sci. Rep.* **63**, 427–464 (2008).
48. Yu, H. L., Liu, X. H., Bi, H. Y. & Chen, L. Q. Deformation behavior of inclusions in stainless steel strips during multi-pass cold rolling. *J. Mater. Process. Technol.* **209**, 455–461 (2009).
49. Yu, H. L., Liu, X. H., Zhao, X. M. & Kusaba, Y. FEM analysis for V-H rolling process by updating geometric method. *J. Mater. Process. Technol.* **180**, 323–327 (2006).
50. Nuruzzaman, D. M. & Chowdhury, M. A. Friction coefficient and wear rate of copper and aluminum sliding against mild steel. *Int. Trans. J. Eng. Manag. Appl. Sci. Technol.* **4**, 29–40 (2013).

Acknowledgments

The lead author gratefully acknowledges the financial support from the Vice-Chancellor's Fellowship Grant and URC small grant at the University of Wollongong, and from the National Natural Science Foundation of China through Grant 51105071.

Author contributions

Y.H. conceived the study. Y.H. wrote the main manuscript text. Y.H., L.X. and K.C. conducted the experiments. Y.H. carried out the FE analysis. Y.H., T.A.K., L.C., G.A., L.H., Q.Q. analyzed the data. All authors reviewed the manuscript.

Additional information

Competing financial interests: The authors declare no competing financial interests.

How to cite this article: YU, H.L. *et al.* A deformation mechanism of hard metal surrounded by soft metal during roll forming. *Sci. Rep.* **4**, 5017; DOI:10.1038/srep05017 (2014).